2024 IEEE International Conference on Robotics and Automation (ICRA 2024)
May 13-17, 2024. Yokohama, Japan

Robotic Constrained Imitation Learning for the Peg Transfer Task in Fundamentals of Laparoscopic Surgery

Kento Kawaharazuka[1], Kei Okada[1], and Masayuki Inaba[1]

***Abstract*— In this study, we present an implementation strategy for a robot that performs peg transfer tasks in Fundamentals of Laparoscopic Surgery (FLS) via imitation learning, aimed at the development of an autonomous robot for laparoscopic surgery. Robotic laparoscopic surgery presents two main challenges: (1) the need to manipulate forceps using ports established on the body surface as fulcrums, and (2) difficulty in perceiving depth information when working with a monocular camera that displays its images on a monitor. Especially, regarding issue (2), most prior research has assumed the availability of depth images or models of a target to be operated on. Therefore, in this study, we achieve more accurate imitation learning with only monocular images by extracting motion constraints from one exemplary motion of skilled operators, collecting data based on these constraints, and conducting imitation learning based on the collected data. We implemented an overall system using two Franka Emika Panda Robot Arms and validated its effectiveness.**

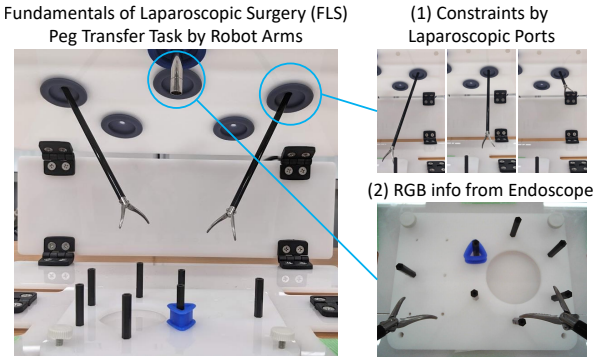

Fig. 1. The concept of this study: regarding peg transfer tasks in Fundamentals of Laparoscopic Surgery (FLS) for robots using imitation learning, we handle two main problems: (1) the forceps are constrained by laparoscopic ports and (2) only RGB information can be obtained from a monocular endoscope.

I. INTRODUCTION

Laparoscopy is a minimally invasive surgical procedure with less scarring and less postoperative pain compared to laparotomy [1], which is highly intriguing as an example of a non-repetitive task required in scientific experiments. In this study, we aim to develop a robot that can perform this laparoscopic surgery autonomously via imitation learning. The nature of laparoscopic surgery, in which an endoscope and forceps are inserted into ports on the body surface, imposes several constraints on the movements of the operator and the robot. They are roughly divided into problem (1) and (2) as shown in Fig. 1: (1) it is necessary to move the forceps using the laparoscopic ports as fulcrums so as not to put load on the ports, and (2) it is difficult to perceive the depth information because images captured by the endoscope are being viewed through a monitor. In this study, we introduce an implementation strategy of a laparoscopic surgical robot that solves these two problems. As a target task, we handle the peg transfer task in Fundamentals of Laparoscopic Surgery (FLS), which is known as an effective training for laparoscopic surgery [2]. While FLS significantly simplifies the actual environment, it captures the overall characteristics of laparoscopic surgery, and we believe that the insights gained here can be effectively utilized.

We introduce several related works. [3] has developed a motion planning method for a suturing surgical robot based on RRT-connect [4] and multiple primitive motions. [5] has discussed a needle guide mechanism and its trajectory optimization for a suturing surgical robot. [6] has proposed a calibration method of da Vinci Research Kit (dVRK) [7] and performed an autonomous debridgment based on stereo image and edge recognition. [8], [9] have discussed surgical action segmentation, and [9] has performed autonomous task execution using the segmentation and model predictive control. In recent years, the application of deep learning to surgical robots has been expanding [10]. [11] has successfully performed a series of laparoscopic surgeries using deep learning-based tissue motion tracking and motion planning. [12] has proposed a method for surgical pattern cutting by applying tension to the gauze based on reinforcement learning. [13] has proposed an eye surgery method using imitation learning. On the other hand, most of them are based on the assumption that a depth image or a model of the target is available. Of course, there are stereoscopic endoscopes, but the basic technique is still based on a monocular image projected on a monitor. The purpose of this study is to address the problems unique to laparoscopic surgery, and to improve the autonomy of the robot based on imitation learning. In particular, we propose and discuss a constrained imitation learning, which solves the difficulty in recognizing depth direction due to monocular images by generating constraints based on a single exemplary demonstration. This is a new approach that does not devise a learning method but devises its data collection based on the extracted constraints, and we show that this approach is useful for laparoscopic surgery. Our contributions are as follows.

- A constrained imitation learning method that collects data with extracted constraints from a single exemplary demonstration and trains a predictive model.
- An overall setup of a laparoscopic surgery robot sys-

[1] The authors are with the Department of Mechano-Informatics, Graduate School of Information Science and Technology, The University of Tokyo, 7-3-1 Hongo, Bunkyo-ku, Tokyo, 113-8656, Japan. [kawaharazuka, k-okada, inaba]@jsk.t.u-tokyo.ac.jp

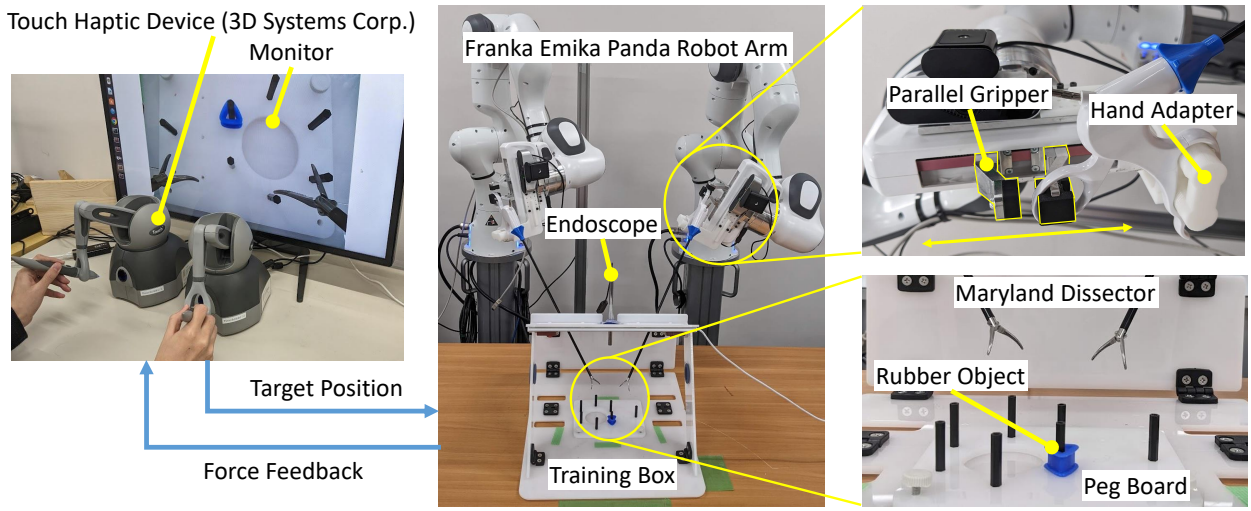

Fig. 2. The setup for robotic peg transfer tasks in Fundamentals of Laparoscopic Surgery. Franka Emika Panda Robot Arms are operated by Touch Haptic Device (3D Systems Corp.). Maryland Dissectors are controlled via Hand Adapter and Parallel Gripper to transfer Rubber Object on Peg Board.

tem and control architecture that can perform the peg transfer task in FLS.

This study is organized as follows. In Section II, we describe the task to be performed, the robot configuration, the experimental environment, inverse kinematics considering constraints on body surface ports, and imitation learning using the data collected considering constraints generated from one exemplary demonstration. In Section III, we describe experiments of constraint generation from one exemplary demonstration, data collection for the peg transfer task with the generated constraints, and the peg transfer experiment based on imitation learning. In Section IV, we discuss the experimental results and limitations of this study, and conclude in Section V.

II. Fundamentals of Laparoscopic Surgery for Robots with Constrained Imitation Learning

A. Fundamentals of Laparoscopic Surgery for Robots

The overall setup of this study is shown in Fig. 2. The robots used in this study are two Franka Emika Panda Robot Arms. A FLS box training kit is placed in front of the robots. A Maryland Dissector is attached to each hand of the robot via a Hand Adapter. A parallel gripper is used to open and close the forceps, and the rotation of forceps in the long axis direction is fixed. The forceps pass through the ports of the box training kit, and rubber object is operated on peg board. Similarly, an endoscope passes through the port and projects the image of the entire peg board on a monitor. Although a peg transfer task is originally performed by moving each rubber object stuck to the six pegs, as a simpler setup, the task in this study is to insert a rubber object stuck to one of the three pegs into the single left peg on the right side from the robot's viewpoint. Two Touch Haptic Devices (3D Systems Corp.) are prepared in front of the monitor for demonstration by experts. The haptic devices can send the target positions of the tips of the forceps to the robot, and at the same time, the forces received by the robot can be reflected to the haptic devices. Note that bilateral control is not performed due to the limitation of the body surface ports and the significant difference in the structure of Touch Haptic Device and Panda Robot Arm.

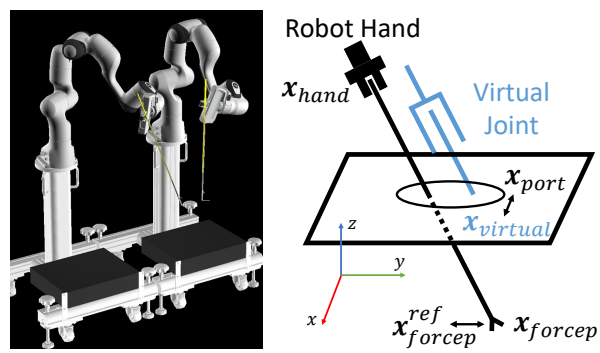

Fig. 3. The configuration to control forceps considering the constraint by a laparoscopic port. The left figure shows a geometric model of robot arms, and the right figure shows the kinematics of forceps with a virtual linear joint from the tip of the hand that overlaps with the long axis of the forceps.

B. Constrained Inverse Kinematics for Laparoscopic Surgery

In laparoscopic surgery, the robot needs to solve inverse kinematics with body surface port constraints. Although a human can sense the constraint appropriately by sensing the force received from the port, it is difficult to do so with the force resolution of Panda Robot Arm and Touch Haptic Device. Therefore, we determine the position of the body surface port in advance and apply the constraint to motion generation. Fig. 3 shows a geometric model of the robot and its constraints. Let $\boldsymbol{x}_{hand}$ denote the coordinate of the robot hand, $\boldsymbol{x}_{forcep}$ denote the tip of the Maryland Dissector, and $\boldsymbol{x}_{port}$ denote the position of the body surface port. Here, the forceps not only rotate but also move in the direction of its long axis, for a total of three degrees of freedom. In order to take this constraint into account, we add a virtual linear joint from the tip of the hand that overlaps with the long axis of the forceps. Let $\boldsymbol{x}_{virtual}$ be the tip of this virtual joint. That

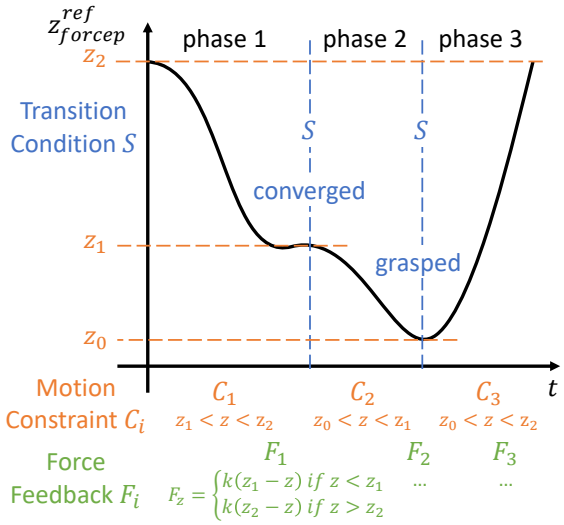

Fig. 4. Trajectory example of target forcep-tip position z^{ref}_{forcep}. The transition condition S divides phases of the demonstration. Motion constraint C_i and force feedback function F_i are generated from the motion in each phase i.

is, given a target value $\boldsymbol{x}^{ref}_{forcep}$ of the forcep-tip position from the haptic device, the following inverse kinematics IK is calculated so that $\boldsymbol{x}_{forcep}$ becomes close to $\boldsymbol{x}^{ref}_{forcep}$ and $\boldsymbol{x}_{virtual}$ becomes close to $\boldsymbol{x}_{port}$,

$$\boldsymbol{\theta}, \boldsymbol{\theta}_{virtual} = \mathrm{IK}(\boldsymbol{x}_{forcep}, \boldsymbol{x}^{ref}_{forcep}, \boldsymbol{x}_{virtual}, \boldsymbol{x}_{port}) \quad (1)$$

where $\boldsymbol{\theta}$ is the joint angle of the robot arm and $\boldsymbol{\theta}_{virtual}$ is the angle of the virtual linear joint.

From now on, the right and left hands are represented in forms such as $\boldsymbol{x}_{hand-left}$ and $\boldsymbol{x}_{forcep-right}$. It may also be expressed in forms such as $x_{hand-right}$ and $z^{ref}_{forcep-left}$ by setting $\boldsymbol{x}^T = \begin{pmatrix} x & y & z \end{pmatrix}$. Note that solving this problem can also be achieved through prioritized inverse kinematics or optimization methods.

C. Constrained Data Collection and Imitation Learning

In order to generate robot motions by imitation learning, we collect human teaching data using haptic devices. However, it is challenging to manipulate the forceps successfully because it is difficult to obtain the depth information. Therefore, we extract constraints on the movement of the forceps from the trajectory of a single slow and accurate exemplary demonstration, and incorporate them to improve the quality of the teaching data and the accuracy of imitation learning. The procedure is as follows.

1) Describe a phase transition condition
2) Extract motion constraints pertaining to each phase from a single exemplary demonstration
3) Collect data by human teaching with force feedback based on the constraints
4) Execute imitation learning based on the collected data

Note that this method is not limited to the FLS task, but can be applied to any task by changing the phase transition condition and motion constraint extraction.

1) Since motion constraint depends on the motion, a long motion must be divided into phases. Therefore, we describe the condition S under which the phase transition or the change in motion constraint occurs. As an example, let us consider the following motions: aligning the forceps to a position slightly above the rubber object, then lowering the forceps, grasping the object, and lifting it up. Here, in order to align the forceps to a position slightly above the object, we can apply a minimum constraint to the z direction after aligning the forceps to the xy direction. In the subsequent motion of lowering the forceps, the minimum value of z is lowered without changing the xy position, and the rubber object becomes graspable. The transition of z^{ref}_{forcep} is shown in Fig. 4. Here, the phase transition condition can be, for example, the opening and closing of the forceps, or the convergence of the motion. That is, if the velocity of $\boldsymbol{x}$ remains small for a certain period of time, it is judged that the positioning has converged and moves on to the next phase, and if a grasping motion occurs, it is judged that the gripper is ready for a lifting motion and moves on to the next phase. Other phase transition conditions can be described in any form, such as the change in distance between the two forceps, reversal of its velocity, state change in the buttons of haptic devices, and so on.

2) Assuming that a single exemplary demonstration is obtained, it is divided into N_C phases by the condition S in 1). From the demonstration in phase i, we extract a motion constraint C_i in phase i ($1 \leq i \leq N_C$). Let us consider the same example as in 1) shown in Fig. 4. In this case, the maximum and minimum value constraints are effective. When $z_{\{0,1,2\}}$ in Fig. 4 is obtained from demonstration, the constraints on z^{ref}_{forcep} in each phase can be described as follows.

$$C_1 : z_1 < z^{ref}_{forcep} < z_2 \quad (2)$$

$$C_2 : z_0 < z^{ref}_{forcep} < z_1 \quad (3)$$

$$C_3 : z_0 < z^{ref}_{forcep} < z_2 \quad (4)$$

Of course, constraints can be imposed on x and y as well, but given the difficulty in recognizing the depth information, constraints on z are the most appropriate. It is possible to extract arbitrary constraints such as the distance between two forceps, the velocity of the forceps, and so on.

3) We incorporate the constraints obtained in 2) into the human teaching as force feedback to the haptic device. For example, if the constraints of Eq. (2) are obtained, the force feedback can be described as follows,

$$F_z = \begin{cases} k_p(z_1 - z^{ref}_{forcep}) & \text{if } z^{ref}_{forcep} < z_1 \\ k_p(z_2 - z^{ref}_{forcep}) & \text{if } z^{ref}_{forcep} > z_2 \end{cases} \quad (5)$$

where F_z is the feedback force of the haptic device in the z direction and k_p is a proportionality constant. This corresponds to applying a feedback control that prevents z from deviating from the range of z_1 and z_2. It is possible to incorporate different constraints by force feedback to F_x and F_y in the same way. After adding these constraints, data is collected by human teaching.

4) Imitation learning is performed based on the collected data. To consider various motion speeds and styles in the

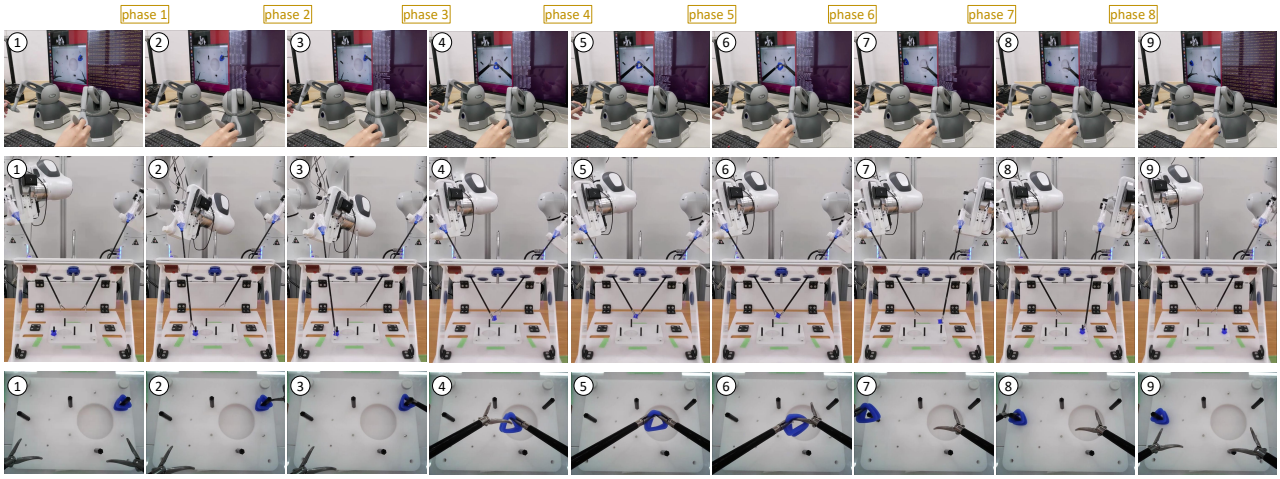

Fig. 5. One exemplary demonstration of peg transfer. The upper figures show the human teaching with haptic devices, the middle figures show the motion of robot arms, and the lower figures show the endoscopic image. Each figure represents the image when there is a phase transition.

human teaching, we use a learnable network input variable called parametric bias [14], [15]. The following predictive model-type network is trained,

$$(\boldsymbol{s}_{t+1}, \boldsymbol{u}_{t+1}) = \boldsymbol{f}(\boldsymbol{s}_t, \boldsymbol{u}_t, \boldsymbol{p}) \tag{6}$$

where t is the current time step, $\boldsymbol{s}$ is the sensor state, $\boldsymbol{u}$ is the control input, $\boldsymbol{p}$ is the parametric bias, and $\boldsymbol{f}$ is the prediction model. In this study, $\boldsymbol{s}$ is $\boldsymbol{\xi}$ ($\in \mathcal{R}^{12}$), which is the image information compressed through AutoEncoder [16]. For $\boldsymbol{u}$, we use the target values of the left and right forceps-tips $\boldsymbol{x}^{ref}_{forcep-\{left,right\}}$ ($\in \mathcal{R}^6$) and the opening and closing state of the forceps $h_{\{left,right\}}$ ($\in \{0,1\}^2$). These data points are acquired at 10 Hz.

For one demonstration k, we obtain the data $D_k = \{(\boldsymbol{s}_1, \boldsymbol{u}_1), (\boldsymbol{s}_2, \boldsymbol{u}_2), \cdots, (\boldsymbol{s}_{T_k}, \boldsymbol{u}_{T_k})\}$ ($1 \leq k \leq K$, where K is the total number of demonstrations and T_k is the number of time steps for the demonstration k). Then, we create the data $D_{train} = \{(D_1, \boldsymbol{p}_1), (D_2, \boldsymbol{p}_2), \cdots, (D_K, \boldsymbol{p}_K)\}$ for training. $\boldsymbol{p}_k$ ($1 \leq k \leq K$) is parametric bias, a learnable input variable for the demonstration k, and the human motion style is self-organized in this space. Using D_{train}, we train Recurrent Neural Network with Parametric Bias (RNNPB) by simultaneously updating the network weight $\boldsymbol{W}$ and each $\boldsymbol{p}_k$. The loss function is a mean squared error, and each $\boldsymbol{p}_k$ is optimized with an initial value of $\boldsymbol{0}$. The execution of the task is simple: the current sensor state $\boldsymbol{s}_t$ and the control input $\boldsymbol{u}_t$ are obtained, $\boldsymbol{u}_{t+1}$ is obtained by calculating Eq. (6), and $\boldsymbol{u}_{t+1}$ is repeatedly commanded to the actual robot. For h, the forceps is closed when the value exceeds 0.5, and opened when the value falls below 0.5. It should be noted that during task execution, $\boldsymbol{p}$ can be arbitrarily set, allowing for variations in motion style [15].

RNNPB consists of 10 layers, which are 4 fully-connected layers, 2 LSTM [17] layers, and 4 fully-connected layers, in order. For the number of units, we set $\{N_u + N_s + N_p$, 500, 300, 100, 100 (number of units in LSTM), 100 (number of units in LSTM), 100, 300, 500, $N_u + N_s\}$ (note that $N_{\{u,s,p\}}$ is the number of dimensions of $\{\boldsymbol{u}, \boldsymbol{s}, \boldsymbol{p}\}$). The activation function is hyperbolic tangent, and the update

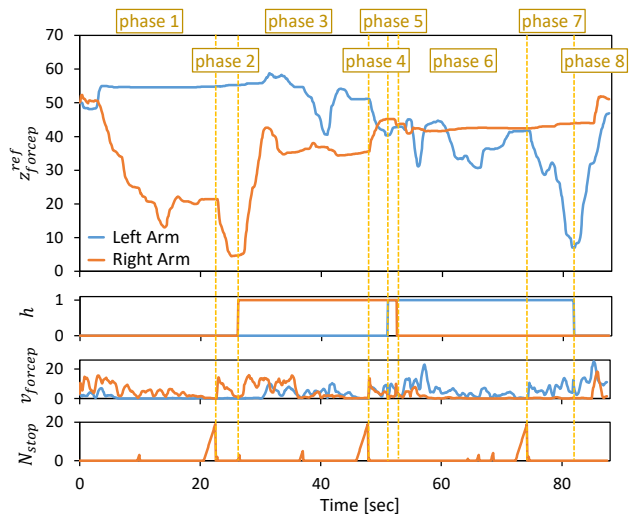

Fig. 6. The transition of z^{ref}_{forcep}, h, and v_{forcep} of the left and right arms, and the transition of N_{stop} for constraint generation from one exemplary demonstration of peg transfer.

rule is Adam [18]. Regarding image compression, for an RGB image of 128×96, convolutional layers of kernel size 3 and stride 2 are applied 5 times, and the number of units is reduced to 1024 and 12 by the fully-connected layers, and then the image is reconstructed by the fully-connected layers and the deconvolutional layers in the same manner. Batch normalization [19] is applied except to the last layer. The activation function is ReLU [20] except for the last layer, which uses Sigmoid. During the training process, random noises are added to the data (improved version of [21]). For $\begin{pmatrix}\boldsymbol{s}^T & \boldsymbol{u}^T\end{pmatrix}^T$, we compute the difference from the previous step and obtain its covariance $\boldsymbol{\Sigma}$. Random numbers following a multivariate normal distribution with mean $\boldsymbol{0}$ and covariance $0.3^2\boldsymbol{\Sigma}$ is added to the data in each step.

III. Experiments

A. Data Collection

First, we make a single exemplary demonstration. In this study, we describe the transition condition S and the motion

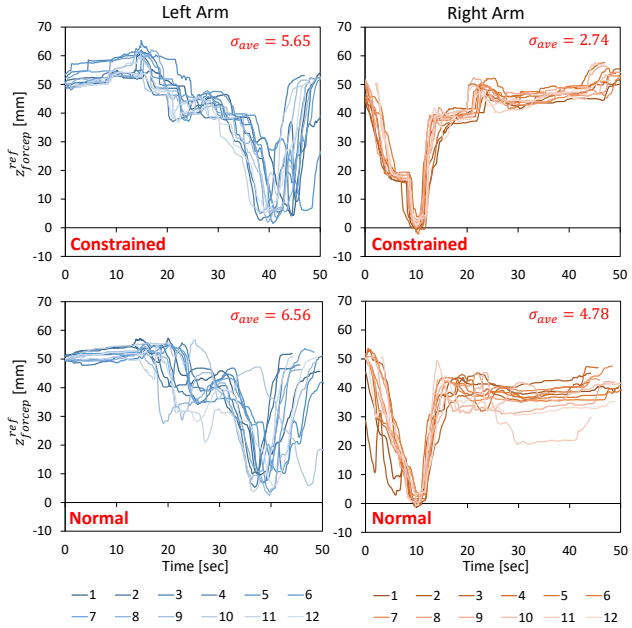

Fig. 7. The transition of z^{ref}_{forcep} of 12 demonstrations of peg transfer with constrained or normal data collection for imitation learning.

constraint C_i in the same way as in the example of Section II-C (Fig. 4). For S, when the state where L2 norm of the forcep-tip velocity $v_{forcep} = ||\dot{\boldsymbol{x}}_{forcep}||_2$ is less than 1.0 regarding both right and left forceps continues for N^{thre}_{stop} steps, or when the opening/closing state h of either left or right forceps changes, the phase is transitioned. Let N_{stop} be the number of consecutive steps in the state where $v_{forcep} < 1.0$ regarding both forceps. We set $N^{thre}_{stop} = 20$ when generating constraints and $N^{thre}_{stop} = 10$ when actually collecting data with the generated constraints. When generating the constraints, the motion itself is not used for learning, so it does not matter how slowly the robot is moved for the single exemplary demonstration. The robot should be moved carefully in the z direction in particular. For C_i, the maximum and minimum values of z^{ref}_{forcep} for the left and right forceps are obtained from the start and end points of the motion in phase i. Since the minimum and maximum values are calculated from the start and end points of the motion phase, we only need to be aware of the phase transition even if the overall motion is unsteady. The phase transition can be viewed visually on the monitor. The demonstration is shown in Fig. 5. The transition of z^{ref}_{forcep}, h, and v_{forcep} of the left and right forceps, and the transition of N_{stop} are shown in Fig. 6. First, we approach the peg in which the rubber object is stuck, aim at the top of the rubber object, grasp it by lowering the right forceps, and lift it up. Next, the left forceps is aimed at the top of the rubber object when it is at the center of the peg board, the left forceps is lowered to grasp it, and the right forceps releases the rubber object. Finally, we aim at the top of the left peg, lower the left forceps and put the rubber object into the peg, then release it and return to the original position. N_{stop} increases when v_{forcep} of the left and right forceps approaches 0, and the phase shifts when N_{stop} reaches N^{thre}_{stop}. The phase is also shifted each time h changes. In the end, $N_C = 8$ phases were generated. From the motion at each phase, the constraint of z^{ref}_{forcep} and the force feedback law based on the constraint are automatically generated.

Next, we collected data for actual imitation learning. The robot performed the action of transferring a rubber object from the right peg to the left peg, for each of the three pegs on the right side, four times each, totaling 12 trials. During this process, data was collected for both constrained data collection (Constrained), where the action was constrained by force feedback, and normal data collection (Normal) without any constraints. The trajectories of $z^{ref}_{forcep-\{left,right\}}$ for the 12 trials are shown in Fig. 7. For both hands, Constrained shows more stable and consistently close values for z^{ref}_{forcep} compared to Normal in each trial. The average variance σ_{ave} for Constrained is 5.65 for the left arm and 2.74 for the right arm, whereas for Normal, it is 6.56 for the left arm and 4.78 for the right arm. Imposing minimum and maximum constraints on the z-directional movement allows for stable data collection.

B. Task Execution with Imitation Learning

Imitation learning was performed using the 12 sets of data collected in Section III-A. The actual task execution using imitation learning with constrained data collection is shown in Fig. 8. Even when the peg that the rubber object is put on is changed in turn, the robot is able to grasp, deliver, and insert the rubber object appropriately. Although the position and the way of holding the rubber object are different in each case, the delivery of the rubber object is successful in all cases.

Next, we compared the imitation learnings based on Constrained and Normal data collection. We conducted a total of 15 experiments, in which the rubber object in each peg was transferred 5 times each. The number of successful cases of (i) taking the rubber object from a peg, (ii) passing the rubber object from the right forceps to the left, and (iii) inserting the rubber object into a peg are shown in Fig. 9. In imitation learning based on Constrained data collection, all operations except for the last insertion have succeeded, and the success rate is very high. On the other hand, in imitation learning based on Normal data collection, there were many cases where the peg was not grasped properly at (i), and the success rate is lower compared to using Constrained data collection. Although the peg's position remains consistent between data collection and this experiment, it is found that the success rate of imitation learning varies significantly depending on the presence or absence of the Constrained data collection.

In addition, for the data of imitation learning based on Constrained and Normal data collection, where the peg that the rubber object is put on is changed in turn, we applied Principle Component Analysis (PCA) to LSTM's latent space and visualized the results in two dimensions in Fig. 10. In both cases, we observed that the latent space evolves in the order of (i) take, (ii) pass, and (iii) insert. Regarding (i), with Constrained data collection, the trajectories of the latent space are distinct for each of the three pegs. However,

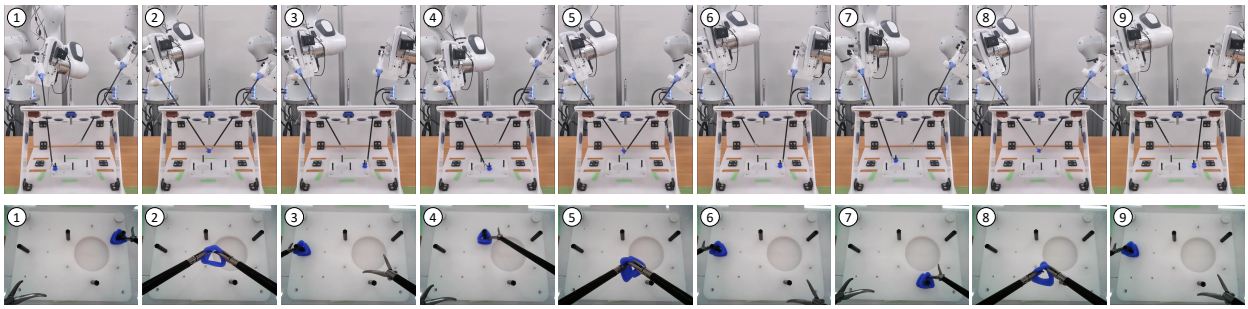

Fig. 8. Peg transfer experiment using imitation learning trained by data obtained with constrained data collection.

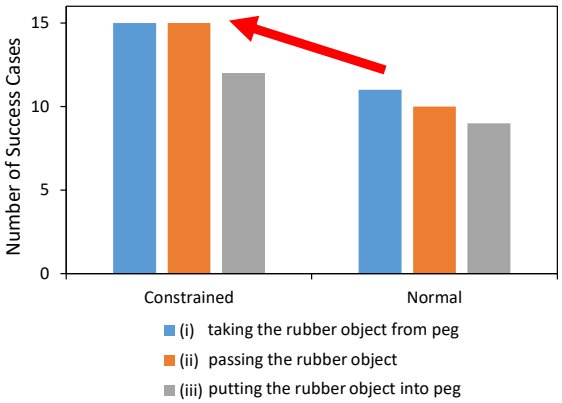

Fig. 9. Comparison of success rates of peg transfer using imitation learning trained by data obtained with constrained or normal data collection.

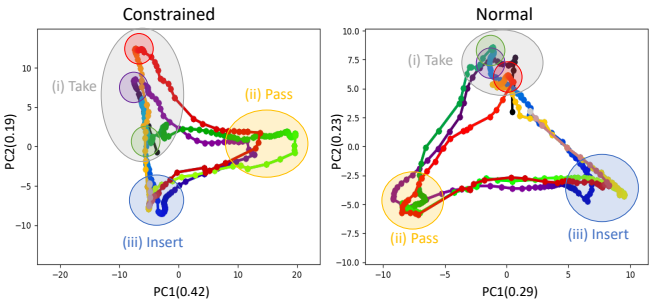

Fig. 10. Comparison of the trajectories of LSTM's latent space when performing peg transfer using imitation learning with constrained or normal data collection. Each graph shows successive peg transfer for three pegs, and the color changes gradually with time.

with Normal data collection, they closely follow the same trajectory. Also, (ii) should exhibit variations in movements depending on how the rubber object is held and where it is passed to, and (iii) should mostly result in similar movements since there is only one peg available. These characteristics are more evident with Constrained data collection, while they are less pronounced with Normal data collection.

IV. Discussion

In this study, we have extracted phase-specific motion constraints from a single exemplary demonstration, and constructed force feedback based on the constraints to overcome the difficulty of motion in the depth direction, especially for a monocular camera. The introduction of motion constraints enables more stable data collection. Imitation learning with the constrained data collection is more stable than imitation learning with the unconstrained data collection, and is able to realize the peg transfer task with higher accuracy.

We discuss the limitations and future prospects of this study. First, it is necessary for humans to appropriately determine which variables to examine for the phase transition and which constraints to generate for each variable. Although this idea itself can be used for various tasks, we believe that the scope of application will be expanded if the system can autonomously determine the phase transition and the form of constraints depending on the task. This is a similar idea to the discovery of the knacks [22]. In the future, we would like to develop a robot that can grow autonomously. Second, in reality, the approach to the inside of the stomach, which is a place with considerable individual differences and gradual changes, requires a more adaptive robot system. Since the current setup is too constrained to operate inside of the stomach, for example, it would be better to apply a constraint only on the distance between the two forceps. There is also the issue of whether the constraints can be determined from a single exemplary demonstration, and further study is needed. Our idea is very simple but effective and can also be used in other fields outside surgery in the future.

V. Conclusion

In this study, we proposed a method to perform the peg transfer task in Fundamentals of Laparoscopic Surgery (FLS) as a setup toward robotic laparoscopic surgery. We developed an overall system which includes two robots with forceps, two haptic devices, and control architecture based on constrained inverse kinematics and constrained imitation learning. In particular, constrained imitation learning allows for easy data collection and precise control using only monocular images, without the need for depth images or models of a target to be operated on. By first generating minimum and maximum constraints for the forceps depth from single exemplary demonstration and collecting data using these constraints for imitation learning, it is possible to easily perform the peg transfer task with higher accuracy. The idea of automatic extraction of motion constraints can be utilized for various robots, tasks, and environments.

Acknowledgement

This work was partially supported by JST Moonshot R&D under Grant Number JPMJMS2033.

REFERENCES

[1] H. C. Clarke, "Laparoscopy–new instruments for suturing and ligation," *Fertility and Sterility*, vol. 23, no. 4, pp. 274–277, 1972.

[2] J. H. Peters, G. M. Fried, L. L. Swanstrom, N. J. Soper, L. F. Sillin, B. Schirmer, K. Hoffman, and the SAGES FLS Committee, "Development and validation of a comprehensive program of education and assessment of the basic fundamentals of laparoscopic surgery," *Surgery*, vol. 135, no. 1, pp. 21–27, 2004.

[3] N. Preda, A. Manurung, O. Lambercy, R. Gassert, and M. Bonfè, "Motion planning for a multi-arm surgical robot using both sampling-based algorithms and motion primitives," in *Proceedings of the 2015 IEEE/RSJ International Conference on Intelligent Robots and Systems*, 2015, pp. 1422–1427.

[4] J. J. Kuffner and S. M. LaValle, "RRT-connect: An efficient approach to single-query path planning," in *Proceedings of the 2000 IEEE International Conference on Robotics and Automation*, 2000, pp. 995–1001.

[5] S. Sen, A. Garg, D. V. Gealy, S. McKinley, Y. Jen, and K. Goldberg, "Automating multi-throw multilateral surgical suturing with a mechanical needle guide and sequential convex optimization," in *Proceedings of the 2016 IEEE International Conference on Robotics and Automation*, 2016, pp. 4178–4185.

[6] D. Seita, S. Krishnan, R. Fox, S. McKinley, J. Canny, and K. Goldberg, "Fast and Reliable Autonomous Surgical Debridement with Cable-Driven Robots Using a Two-Phase Calibration Procedure," in *Proceedings of the 2018 IEEE International Conference on Robotics and Automation*, 2018, pp. 6651–6658.

[7] P. Kazanzides, Z. Chen, A. Deguet, G. S. Fischer, R. H. Taylor, and S. P. DiMaio, "An open-source research kit for the da Vinci Surgical System," in *Proceedings of the 2014 IEEE International Conference on Robotics and Automation*, 2014, pp. 6434–6439.

[8] D. Meli and P. Fiorini, "Unsupervised Identification of Surgical Robotic Actions From Small Non-Homogeneous Datasets," *IEEE Robotics and Automation Letters*, vol. 6, no. 4, pp. 8205–8212, 2021.

[9] G. D. Rossi, M. Minelli, S. Roin, F. Falezza, A. Sozzi, F. Ferraguti, F. Setti, M. Bonfè, C. Secchi, and R. Muradore, "A First Evaluation of a Multi-Modal Learning System to Control Surgical Assistant Robots via Action Segmentation," *IEEE Transactions on Medical Robotics and Bionics*, vol. 3, no. 3, pp. 714–724, 2021.

[10] I. Rivas-Blanco, C. J. Pérez-Del-Pulgar, I. García-Morales, and V. F. Muñoz, "A Review on Deep Learning in Minimally Invasive Surgery," *IEEE Access*, vol. 9, pp. 48 658–48 678, 2021.

[11] H. Saeidi, J. D. Opfermann, M. Kam, S. Wei, S. Leonard, M. H. Hsieh, J. U. Kang, and A. Krieger, "Autonomous robotic laparoscopic surgery for intestinal anastomosis," *Science Robotics*, vol. 7, no. 62, p. eabj2908, 2022.

[12] B. Thananjeyan, A. Garg, S. Krishnan, C. Chen, L. Miller, and K. Goldberg, "Multilateral surgical pattern cutting in 2D orthotropic gauze with deep reinforcement learning policies for tensioning," in *Proceedings of the 2017 IEEE International Conference on Robotics and Automation*, 2017, pp. 2371–2378.

[13] J. W. Kim, P. Zhang, P. Gehlbach, I. Iordachita, and M. Kobilarov, "Towards Autonomous Eye Surgery by Combining Deep Imitation Learning with Optimal Control," in *Proceedings of the 2020 Conference on Robot Learning*, 2021, pp. 2347–2358.

[14] J. Tani, "Self-organization of behavioral primitives as multiple attractor dynamics: a robot experiment," in *Proceedings of the 2002 International Joint Conference on Neural Networks*, 2002, pp. 489–494.

[15] K. Kawaharazuka, Y. Kawamura, K. Okada, and M. Inaba, "Imitation Learning with Additional Constraints on Motion Style using Parametric Bias," *IEEE Robotics and Automation Letters*, vol. 6, no. 3, pp. 5897–5904, 2021.

[16] G. E. Hinton and R. R. Salakhutdinov, "Reducing the Dimensionality of Data with Neural Networks," *Science*, vol. 313, no. 5786, pp. 504–507, 2006.

[17] S. Hochreiter and J. Schmidhuber, "Long short-term memory," *Neural computation*, vol. 9, no. 8, pp. 1735–1780, 1997.

[18] D. P. Kingma and J. Ba, "Adam: A Method for Stochastic Optimization," in *Proceedings of the 3rd International Conference on Learning Representations*, 2015, pp. 1–15.

[19] S. Ioffe and C. Szegedy, "Batch Normalization: Accelerating Deep Network Training by Reducing Internal Covariate Shift," in *Proceedings of the 32nd International Conference on Machine Learning*, 2015, pp. 448–456.

[20] V. Nair and G. E. Hinton, "Rectified Linear Units Improve Restricted Boltzmann Machines," in *Proceedings of the 27th International Conference on Machine Learning*, 2010, pp. 807–814.

[21] P. Florence, L. Manuelli, and R. Tedrake, "Self-Supervised Correspondence in Visuomotor Policy Learning," *IEEE Robotics and Automation Letters*, vol. 5, no. 2, pp. 492–499, 2020.

[22] Y. Kuniyoshi, Y. Ohmura, K. Terada, A. Nagakubo, S. Eitoku, and T. Yamamoto, "Embodied basis of invariant features in execution and perception of whole-body dynamic actions – knacks and focuses of Roll-and-Rise motion," *Robotics and Autonomous Systems*, vol. 48, no. 4, pp. 189–201, 2004.